Int. J. Solids Structures Vol. 29, No. 14/15, pp. 1763–1779, 1992
Printed in Great Britain.

0020–7683/92 $5.00 + .00
Pergamon Press plc

WAVE PROPAGATION IN DAMAGED SOLIDS

D. GROSS and CH. ZHANG†
Institute of Mechanics, TH Darmstadt, Germany

Abstract—In this paper, a theoretical model is presented for investigating elastic wave propagation in damaged solids. This model is suited for damaged solids with dilutely distributed defects, and it may aid in the design of experimental configurations and in the proper interpretation of measured data from ultrasonic non-destructive evaluation (NDE) for detecting and characterizing the damage states of the solid. The problem of wave scattering by a single defect of arbitrary shape is first formulated as a set of boundary integral equations, whose solution yields the unknown quantities on the boundary of the defect. The scattering cross-section is then introduced as a measure of the overall effects of the defect on the energy withdrawal from the incident wave. The damaged solid is approximated by an equivalent effective medium which is thought of as statistically homogeneous and linearly viscoelastic. By introducing a complex wave number, neglecting interaction effects among individual defects, and using energy considerations, a simple equation is obtained for calculating the attenuation coefficient from the average scattering cross-section and the number density of the defects. Kramers–Kronig relations are subsequently applied to compute the effective wave (phase) velocity from which the group velocity can be immediately calculated. A method for finding the dynamic effective stiffness of the damaged solid from the attenuation coefficient and the effective wave velocity is proposed. Numerical results are presented for a damaged solid permeated by a distribution of completely randomly oriented penny-shaped microcracks.

1. INTRODUCTION

Wave propagation in a damaged solid, unlike in an ideally perfect solid, is generally accompanied by attenuation and dispersion. Attenuation refers to the diminishing of wave intensity or wave amplitude as a wave propagates through a damaged medium, while dispersion refers to the shape distortion of a wave due to the frequency dependence of the effective wave (phase) velocity. Both attenuation and phase velocity are measurable quantities, and the amount of change in the attenuation and phase velocity can be correlated to the level of damage states. This feature has been advantageously exploited in ultrasonic nondestructive evaluation (NDE) relying on wave propagation in solids, which provides an ideal means for detecting and characterizing flaws in a damaged solid. Techniques utilizing ultrasonic waves are especially appealing because of the direct connection between the characteristics of the wave propagation and the damage states of a solid (e.g. Achenbach, 1990). This paper aims at providing a theoretical model which may aid in the design of experimental configurations and in the proper interpretation of measured data.

There are many factors affecting wave attenuation and dispersion, such as spreading of a wave beam, scattering, absorption due to various mechanisms and mode conversion resulting in partitioning of the energy among two or more wave modes each traveling at its own velocity. The present analysis only considers the scattering effects of distributed damages, since scattering is a common cause of attenuation of acoustic energy. During the scattering processes, part of the incident wave energy is converted into the energy of scattered waves. Consequently, a perfectly elastic and damaged solid is seen by an incident wave as an attenuative and dispersive medium, despite the conservative nature of the entire system and its constituents. It is not easy to define precisely the terminology "damage". In this paper, "damage" is defined as a collection of micro-heterogeneities whose presence gives rise to changes of the overall material properties, such as stiffness, strength and anisotropy. This definition may be misleading in the case of stiffer inhomogeneities such as in particle-reinforced composites. Here, a stiffening effect emerges which is desirable from the engineering point of view. Even in this case, the inhomogeneities are regarded as "damage", since their presence will change the material properties and thus the wave

† On leave from: Department of Engineering Mechanics, Tongji University, Shanghai 200092, China.

propagation characteristics (attenuation and phase velocity). In a real situation, scattering by the material microstructure such as grain boundaries and second phase particles may also have strong influence on wave attenuation and dispersion. In this analysis, this contribution is ignored by assuming that the wave length and the characteristic dimensions of the defects are sufficiently larger than the characteristic dimensions of the material microstructure.

An extensive literature exists on wave propagation in multi-phase materials, especially in particulate composites (e.g. Mal and Knopoff, 1967; McCoy, 1973; Bose and Mal, 1974; Kuster and Toksoz, 1974; Kinra *et al.*, 1976; Varadan and Varadan, 1979; Sayers, 1980; Kinra and Anaud, 1982; Sayers and Smith, 1983; Datta *et al.*, 1988; Ledbetter and Datta, 1986; Sabina and Willis, 1988) and in voided materials (e.g. Varadan *et al.*, 1978; Sayers, 1981; Sayers and Smith, 1981; Gubernatis and Domany, 1984; Varadan *et al.*, 1985; Lewandowski, 1987a,b; Stigh, 1987). It is not the goal of this paper to give a comprehensive review on this subject, and for detail we refer to the above-mentioned works and references cited therein. There are also several investigations on wave propagation in solids containing cracks (e.g. Anderson *et al.*, 1974; O'Connell and Budiansky, 1974; Piau, 1979, 1980; Chatterjee *et al.*, 1980; Hudson, 1981, 1986; McCarthy and Carroll, 1984; Zhang and Achenbach, 1991). Most of these investigations used either the formalism of Foldy (1949) or the quasicrystalline approximation of Lax (1952). Also, most works were restricted to Rayleigh regime where the wave length is considerably larger than the characteristic dimension of the defects, or to the diffusive regime for the opposite case. Few works have been devoted to the stochastic regime where the wave length and the characteristic dimensions of the defect are of the same order. As a consequence of the Rayleigh or low-frequency approximation the phase velocity does not exhibit frequency dependence, and it does not correctly describe the dispersion behavior of the wave. Kramers–Kronig relations have been successfully applied by Beltzer and co-workers for studying wave attenuation and dispersion in particle-reinforced composites, and the essential results have been reviewed by Beltzer (1988, 1989). This causal approach has been recently extended to surface-crack problems by Zhang and Achenbach (1990), to solids containing parallel anti-plane cracks by Angel and Achenbach (1990), and to randomly and non-randomly cracked 2- or 3-D solids by Zhang and Gross (1991a). The essential advantage of this approach is that it puts no limitations on frequency, and it requires only a few parameters describing the statistical distribution and orientation of the microdefects. In this paper, this approach is further extended to damaged solids with dilutely distributed defects of arbitrary shapes. The procedure for calculating the attenuation coefficient and the phase velocity is essentially the same as in our previous works (e.g. Zhang and Gross, 1991a). In the present analysis, however, the group velocity is also computed, and a method for finding the dynamic effective stiffness of the damaged solid is proposed. As an example, numerical results are presented for a damaged solid permeated by a distribution of completely randomly oriented penny-shaped microcracks.

2. SCATTERING CROSS-SECTION OF A SINGLE DEFECT

We consider an infinite, homogeneous, isotropic and linearly elastic solid containing a volumetric defect of arbitrary shape as shown in Fig. 1a. The defect is assumed to be also

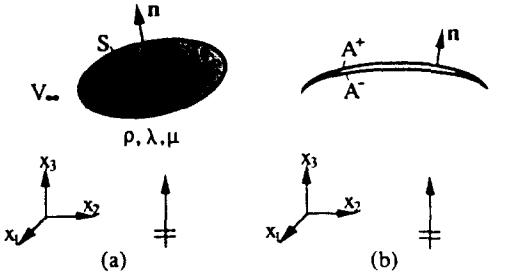

Fig. 1. (a) Volumetric defect. (b) Crack.

homogeneous, isotropic, and linearly elastic, and it occupies the domain V_D inside a sufficiently regular, bounded, and closed surface S. The material constants of the defect are characterized by ρ^0, λ^0 and μ^0, while ρ, λ and μ represent the corresponding material constants of the matrix. Here, a defect is defined, though not precisely, as an inhomogeneity whose material constants differ from those of the matrix, and whose presence will disturb wave propagation in the matrix material. Depending on the relative stiffness of the defect to that of the matrix, the defect can be used to model the fibers in a particle-reinforced composite, the localized damaged zone in an otherwise perfect material, or a void. A crack is also contained as a limit-case. Although interface flaws such as interface cracks, interface debonding, interface sliding and interface layer (interphase) could be present in a real situation (e.g. Aboudi, 1988; Datta *et al.*, 1988), it is assumed here that a perfect bonding between the matrix and the inhomogeneity prevails. Interface flaws can be easily taken into account in the formulation. As an incident wave impinges on the defect, scattered waves are generated. The total wave field in V_∞ can be written as a sum of the incident wave field and the scattered wave field:

$$u_i = u_i^{in} + u_i^{sc}, \quad \sigma_{ij} = \sigma_{ij}^{in} + \sigma_{ij}^{sc}. \tag{1}$$

The incident wave field, u_i^{in} and σ_{ij}^{in}, is defined as the wave field that would be present if the defect were absent. The scattered wave field, u_i^{sc} and σ_{ij}^{sc}, is induced by the interaction of the incident wave with the defect. The incident wave field is defined in the entire space $V = V_D + V_\infty$, while the scattered wave field is only defined in V_∞. The solid is assumed to be in time-harmonic motion, but the common term $e^{-i\omega t}$ is suppressed throughout the analysis, where ω is the angular frequency. Both the total wave field and the partial wave fields satisfy the equations of motion

$$\sigma_{ij,j} + \rho\omega^2 u_i = 0, \tag{2}$$

the linear kinematic equation

$$\varepsilon_{ij} = \tfrac{1}{2}(u_{i,j} + u_{j,i}), \tag{3}$$

the Hooke's Law

$$\sigma_{ij} = E_{ijkl}\varepsilon_{kl}, \tag{4}$$

and the boundary (continuity) conditions

$$u_i^0(\mathbf{x}) = u_i(\mathbf{x}), \quad \mathbf{x} \in S, \tag{5}$$

$$\sigma_{ij}^0 n_j(\mathbf{x}) = \sigma_{ij} n_j(\mathbf{x}), \quad \mathbf{x} \in S. \tag{6}$$

Here and in the following, the superscript 0 designates quantities in V_D, and n_j denotes the components of the unit normal vector of S pointing into the interior of V_∞. For isotropic solids, E_{ijkl} can be written as

$$E_{ijkl} = \lambda\delta_{ij}\delta_{kl} + \mu(\delta_{ik}\delta_{jl} + \delta_{il}\delta_{jk}), \tag{7}$$

where δ_{ij} represents the Kronecker delta. Replacing the material constants of the matrix by the corresponding material constants of the defect, similar equations like (2)–(4) can be written for the displacement and the stress field in V_D, i.e. u_i^0 and σ_{ij}^0. However, these equations are not given here for the sake of brevity.

While the boundary conditions (5) and (6) are generally valid, some modifications have to be made for certain limit-cases. For instance, the boundary conditions should read for a rigid defect:

$$u_i(\mathbf{x}) = \text{const.}, \quad \mathbf{x} \in S; \tag{8}$$

for a vacant void:

$$\sigma_{ij} n_j(\mathbf{x}) = 0, \quad \mathbf{x} \in S; \tag{9}$$

and for a fluid-saturated void:

$$u_n^0(\mathbf{x}) = u_n(\mathbf{x}), \quad \mathbf{x} \in S, \tag{10}$$

$$f_n^0(\mathbf{x}) = f_n(\mathbf{x}), \quad f_t^0(\mathbf{x}) = f_t(\mathbf{x}) = 0, \quad \mathbf{x} \in S. \tag{11}$$

In eqns (10) and (11), n and t denote the normal and the tangential components of the displacements and the tractions. For a traction-free crack, the boundary conditions are

$$\sigma_{ij} n_j(\mathbf{x}) = 0, \quad \mathbf{x} \in A, \tag{12}$$

where $A = A^+ + A^-$ denotes the surface of the crack (see Fig. 1b). In this analysis, the incident wave field is assumed to be known a priori, and the scattered wave field has to be determined, which satisfies the radiation conditions at infinity. By using the elastodynamic representation theorem, the wave field in V_D and the scattered wave field in V_∞ can be expressed as

$$u_i^0(\mathbf{x}) = -\int_S [\sigma_{ijk}^{G_0}(\mathbf{x};\mathbf{y}) u_i^0(\mathbf{y}) - u_{ik}^{G_0}(\mathbf{x};\mathbf{y}) \sigma_{ij}^0(\mathbf{y})] n_j \, dS, \quad \mathbf{x} \in V_D, \tag{13}$$

$$u_i^\infty(\mathbf{x}) = \int_S [\sigma_{ijk}^{G}(\mathbf{x};\mathbf{y}) u_i(\mathbf{y}) - u_{ik}^{G}(\mathbf{x};\mathbf{y}) \sigma_{ij}(\mathbf{y})] n_j \, dS, \quad \mathbf{x} \in V_\infty, \tag{14}$$

where $\mathbf{x}$ and $\mathbf{y}$ denote the position vectors of the observation point and the source point, and $u_{ik}^{G_0}$, $\sigma_{ijk}^{G_0}$ and u_{ik}^{G}, σ_{ijk}^{G} represent the displacement and the stress Green's functions of the defect and the matrix, respectively.

Using eqns (13) and (14), taking the limit $\mathbf{x} \to S$, and considering the boundary conditions (5) and (6), a system of coupled boundary integral equations (BIEs) can be obtained as

$$\tfrac{1}{2} u_k(\mathbf{x}) = -\int_S [\sigma_{ijk}^{G_0}(\mathbf{x};\mathbf{y}) u_i(\mathbf{y}) - u_{ik}^{G_0}(\mathbf{x};\mathbf{y}) \sigma_{ij}(\mathbf{y})] n_j \, dS, \quad \mathbf{x} \in S, \tag{15}$$

$$\tfrac{1}{2} u_k(\mathbf{x}) - u_k^{in}(\mathbf{x}) = \int_S [\sigma_{ijk}^{G}(\mathbf{x};\mathbf{y}) u_i(\mathbf{y}) - u_{ik}^{G}(\mathbf{x};\mathbf{y}) \sigma_{ij}(\mathbf{y})] n_j \, dS, \quad \mathbf{x} \in S, \tag{16}$$

where the integrals are understood as Cauchy principal value integrals.

The boundary integral equations (15) and (16) are valid for arbitrarily shaped defects. Implications arise when the defect takes the form of a crack with vanishing thickness. In this case, the usual displacement BIE formulation degenerates, and it is convenient to use the traction BIE formulation. For a three-dimensional crack of arbitrary shape, a non-hypersingular BIE formulation leads to the following traction BIEs (e.g. Zhang and Gross, 1991b)

$$f_p^m(\mathbf{x}) = E_{pqkl} n_q(\mathbf{x}) \left\{ \varepsilon_{rst} \varepsilon_{rlj} \int_{A^+} \sigma_{ijk}^{G}(\mathbf{x};\mathbf{y}) \Delta u_{i,t}(\mathbf{y}) n_s - \rho\omega^2 \int_{A^+} u_{ik}^{G}(\mathbf{x};\mathbf{y}) \Delta u_i(\mathbf{y}) n_l \, dS \right\}, \quad \mathbf{x} \in A^+, \tag{17}$$

where ε_{rst} is the permutation tensor, and Δu_i are the crack opening displacements. Also here, the integrals are understood as Cauchy principal value integrals.

The boundary integral equations (15)–(17) can be solved numerically by adopting the boundary element method (BEM). Special care must be taken to account for the singularities arising in the Green's functions. For crack problems, additional singularities occur at the tips of the crack which should be modeled properly. Once the quantities on the boundary of the defect have been calculated by solving eqns (15) and (16) (or eqn (17)), the displacement and the stress field at any internal point can be determined by using the respective representation formulas for these quantities.

In this analysis, the incident wave is taken to be either a plane time-harmonic longitudinal wave (L-wave) of the form

$$u_k^{\text{in}}(\mathbf{x}, t) = U_k^{\text{L}} e^{i(k_{\text{L}} x_j n_j - \omega t)}, \tag{18}$$

or a plane time-harmonic transverse wave (TV-wave) of the form

$$u_k^{\text{in}}(\mathbf{x}, t) = U_k^{\text{T}} e^{i(k_{\text{T}} x_j n_j - \omega t)}, \tag{19}$$

where n_j are the components of the wave propagation vector $\mathbf{n}$, U_k^{L} and U_k^{T} are the amplitudes, and k_{L} and k_{T} are the wave numbers of the incident L- and TV-waves, respectively. The presence of a defect gives rise to a perturbation of the intensity of the incident wave, since a part of the energy of the incident wave is converted into the energy of scattered waves. To describe the effects of the defect on the energy withdrawal from the incident wave, the scattering cross section γ is introduced as

$$\gamma = \frac{\langle P^{\text{sc}} \rangle}{\langle I \rangle}, \tag{20}$$

where $\langle P^{\text{sc}} \rangle$ represents the time-averaged energy flow of scattered waves over a period $T = 2\pi/\omega$, and $\langle I \rangle$ denotes the time-averaged intensity of the incident wave. For an incident plane time-harmonic L-wave defined by eqn (18) the time-averaged wave intensity is given by

$$\langle I \rangle = \frac{\rho \omega^3}{2k_{\text{L}}} U_k^{\text{L}} U_k^{\text{L}*}, \tag{21}$$

while for an incident plane time-harmonic TV-wave of the form (19) $\langle I \rangle$ is determined by

$$\langle I \rangle = \frac{\rho \omega^3}{2k_{\text{T}}} U_k^{\text{T}} U_k^{\text{T}*}, \tag{22}$$

where asterisk stands for the complex conjugate. The time-averaged energy flow of the scattered waves $\langle P^{\text{sc}} \rangle$ can be expressed as

$$\langle P^{\text{sc}} \rangle = -\tfrac{1}{2} \operatorname{Re}\left[i\omega \int_S \sigma_{ij}^{\text{sc}} (u_i^{\text{sc}})^* n_j \, \mathrm{d}S \right]. \tag{23}$$

If the defect is a crack, eqn (23) can be recast into the following form:

$$\langle P^{\text{sc}} \rangle = \tfrac{1}{2} \operatorname{Re}\left[i\omega \int_{A^+} \sigma_{ij}^{\text{in}} \Delta u_i^* n_j \, \mathrm{d}S \right]. \tag{24}$$

The time-averaged energy flow $\langle P^{\text{sc}} \rangle$ describes the energy scattered in all directions and, thus, lost by an incident wave at the expense of its interaction with the crack.

The scattering cross-section γ is of particular importance to the present analysis, and it is directly related to the attenuation coefficient, as will be shown in the following section.

3. DISTRIBUTED DEFECTS AND ATTENUATION COEFFICIENT

We consider now a distribution of microdefects embedded in a homogeneous, isotropic and linearly elastic solid, as shown in Fig. 2a. Depending on the statistical distribution and orientation of the dispersed microdefects, the overall behavior of the damaged solid may exhibit macroscopic anisotropy or isotropy. Wave propagation in such a heterogeneous medium is very complex, and it is impractical, often also impossible, to study the local events near individual defects. Often, it suffices to describe the overall average response of the material. One approach for doing this is the so-called effective medium approach, which has been extensively used in the literature. Here, we will adopt this approach for analyzing the dynamic behavior of the damaged solid. To be more specific, let us consider a representative volume element (RVE) as shown in Fig. 2b, which is large enough compared to the characteristic dimensions of the material microstructure including the microdefects, but small enough compared to the characteristic dimensions of the damaged solid. Wave propagation in this heterogeneous RVE involves wave scattering due to the presence of the defects, which withdraws the energy of the incident wave. Consequently, the wave intensity decreases or attenuates, though the matrix and the defects are perfectly elastic and do not dissipate energy. Also, the presence of the damage will change the effective wave velocity, which is now frequency dependent. These two phenomena, referred to as wave attenuation and dispersion, are very similar to those of wave propagation in a homogeneous and linearly viscoelastic medium. Because of this similarity, it is intuitive to replace the originally heterogeneous RVE by an equivalent effective medium (EEM) which is thought of as homogeneous and linearly viscoelastic (see Fig. 2c). This procedure, often termed "homogenization" technique, relies on the assumption that both the originally damaged RVE and the undamaged EEM should have, at least approximately, the same response under the same dynamic loading conditions. In principle, we can first determine the dynamic effective material constants, and then calculate the corresponding wave propagation characteristics (attenuation and phase velocity). Here, we follow an opposite way which appears to be more convenient as will be shown in the following.

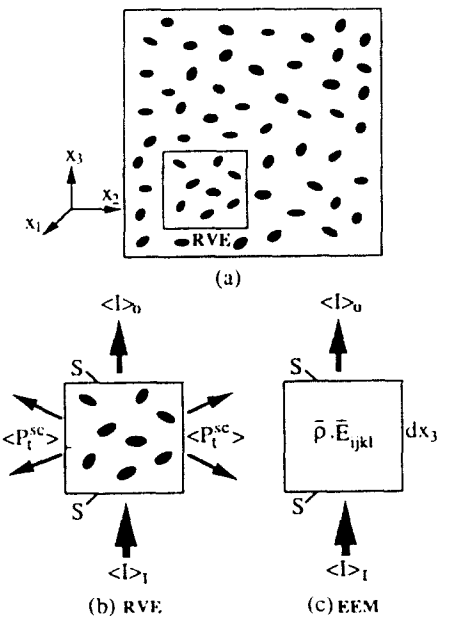

Fig. 2. (a) Damaged solid. (b) Representative volume element (RVE). (c) Equivalent effective medium (EEM).

For simplicity, let us consider a plane time-harmonic wave propagating in the positive x_3-direction. Suppose that the input wave energy at the bottom side of the RVE is $S\langle I\rangle_1$, and the output wave energy at the top side is $S\langle I\rangle_0$, then the energy balance provides

$$S\langle I\rangle_0 = S\langle I\rangle_1 - \langle P_i^{sc}\rangle, \tag{25}$$

where S denotes the surface of the bottom and the top side of the RVE, and $\langle P_i^{sc}\rangle$ is the total energy loss due to the interaction of the incident wave with the defects within the RVE

$$\langle P_i^{sc}\rangle = \sum_{i=1}^{N} \langle P_i^{sc}\rangle, \tag{26}$$

where the sum extends over all the defects in the RVE. In general, it is very difficult to determine the total energy loss $\langle P_i^{sc}\rangle$ exactly, since multiple scattering processes take place. To simplify our analysis, we adopt here the dilute approximation which neglects interaction or multiple scattering effects between individual microdefects. In this case, the total energy loss may be approximated by

$$\langle P_i^{sc}\rangle \approx N\{\gamma\}\langle I(\mathbf{x},\omega)\rangle, \tag{27}$$

in which $\{\gamma\}$ is the average scattering cross-section with respect to defect size and orientation. Substitution of (27) into (25) yields

$$\langle I\rangle_0 = \langle I\rangle_1 - \frac{N}{S}\{\gamma\}\langle I(\mathbf{x},\omega)\rangle. \tag{28}$$

We go on to consider the homogeneous and linearly viscoelastic EEM (see Fig. 2c). Wave propagation in this medium can be conveniently described by a complex wave number

$$K(\omega) = \frac{\omega}{\tilde{c}(\omega)} + i\alpha(\omega), \tag{29}$$

where $\tilde{c}(\omega)$ is the effective wave (phase) velocity and $\alpha(\omega)$ is the attenuation coefficient. With (29), a plane time-harmonic viscoelastic wave propagating in the positive x_3-direction can be expressed as

$$u_k(\mathbf{x},\omega) = U_k(\omega)e^{i[K(\omega)x_3 - \omega t]} = U_k(\omega)e^{-\alpha x_3}e^{i\omega[x_3/\tilde{c}(\omega) - t]}, \tag{30}$$

in which $U_k(\omega)$ is an amplitude factor. With a positive α, eqn (30) describes a plane time-harmonic wave with diminishing amplitudes. The time-averaged intensity of this wave can be written as

$$\langle I(\mathbf{x},\omega)\rangle = \langle I(\mathbf{x},\omega)\rangle_1 e^{-2\alpha x_3}, \tag{31}$$

which leads to

$$\frac{\partial\langle I\rangle}{\partial x_3} = -2\alpha\langle I(\mathbf{x},\omega)\rangle. \tag{32}$$

Thus, the wave intensity at the top side of the EEM is

$$\langle I(\mathbf{x},\omega)\rangle_0 = \langle I(\mathbf{x},\omega)\rangle_1 + \frac{\partial\langle I\rangle}{\partial x_3}\,\mathrm{d}x_3 = \langle I\rangle_1 - 2\alpha\langle I(\mathbf{x},\omega)\rangle\,\mathrm{d}x_3. \tag{33}$$

Since the output wave energy at the top side of the originally damaged RVE should equal that of the homogenized undamaged EEM, we obtain by equating (28) and (33):

$$\alpha = \tfrac{1}{2}n\{\gamma\}, \tag{34}$$

where $n = N\,(\mathrm{d}x_3 S)$ represents the number density of the defects (number of defects per unit volume). Equation (34) implies that the attenuation coefficient α is simply determined by the average scattering cross-section $\{\gamma\}$ and the number density n of the defects. The weakness of this formulation is clearly the neglect of the interaction effects between individual defects, which become increasingly important as the defect density n increases. Thus, the present formulation is only valid for dilutely distributed damages, and it is less favourable for large damage concentrations. Interaction effects can be taken into account approximately by adopting the differential scheme developed by Beltzer (1988, 1989) or by using the method applied by Zhang and Achenbach (1991). This will, however, make the present analysis too cumbersome, and we will leave this work for future research. The essential advantage of the present formulation is that we can determine the attenuation coefficient α by using a very simple formula (34), rather than have to resort to other complicated methods.

Another point to mention is that the contributions from wave scattering by other material microstructure, such as grain boundaries and second phase particles etc. are ignored in this analysis. This is less crucial if we assume that the wave length and the characteristic dimensions of the defects are sufficiently large compared to the characteristic dimensions of the material microstructure.

4. PHASE VELOCITY AND GROUP VELOCITY

As mentioned in the previous section, the effective medium of the damaged solid is thought of as statistically homogeneous and linearly viscoelastic. In this section, we further assume that the effective medium is causal and passive. These assumptions are certainly acceptable from the physical point of view. As a consequence of the linearity, the causality and the passivity of the effective medium, the real part and the imaginary part of the complex wave number are independent of one another, and they are related by Kramers–Kronig relations (e.g. Kronig, 1926; Kramers, 1927). These relations enable us to determine the effective wave (phase) velocity, once the attenuation coefficient has been calculated from eqn (34). Since detailed derivation and discussion of Kramers–Kronig relations can be found in many references (e.g. Beltzer, 1988; Golden and Graham, 1988; Zhang and Gross, 1991a), here we only summarize the essential results.

The linearity of the effective medium ensures that the superposition principle applies. The causality condition implies that the current overall average response of the effective medium is affected only by past and contemporaneous events, i.e.

$$\bar{\eta}_{ijkl}(t-\tilde{t}) = 0, \quad \text{for} \quad t \leqslant \tilde{t}, \tag{35}$$

where $\bar{\eta}_{ijkl}(t-\tilde{t})$ is the effective, real-valued and time-dependent stiffness tensor. Consequently, we have

$$\tau_{ij}(\mathbf{x},t) = \int_{-\infty}^{t} \bar{\eta}_{ijkl}(t-\tilde{t})\gamma_{kl}(\mathbf{x},\tilde{t})\,\mathrm{d}\tilde{t}, \tag{36}$$

where $\tau_{ij}(\mathbf{x},t)$ and $\gamma_{ij}(\mathbf{x},t)$ are the ensemble average of the stress and the strain components. It should be noted here that the Fourier transforms of $\tau_{ij}(\mathbf{x},t)$, $\gamma_{ij}(\mathbf{x},t)$ and $\bar{\eta}_{ijkl}(t)$, i.e. $\sigma_{ij}(\mathbf{x},\omega)$, $\varepsilon_{ij}(\mathbf{x},\omega)$ and $\bar{E}_{ijkl}(\omega)$, still satisfy the equations of motion (2), the kinematic

equation (3) and the constitutive equation (4) as in the linearly elastic case. However, the material constants in these equations should be replaced by the corresponding effective material constants, which are in general frequency dependent.

The passivity condition means physically that no energy can be created within the effective medium, which may be stated mathematically as

$$\mathrm{Im}\,(\bar{E}_{ijkl}\varepsilon_{ij}^{*}\varepsilon_{kl}) \leqslant 0. \tag{37}$$

The passivity condition (37) leads to

$$\mathrm{Im}\,[K(\omega)] \leqslant 0, \quad \text{or} \quad \alpha \geqslant 0, \tag{38}$$

which could be expected from the physical point of view that only with a positive α will eqn (30) describe a plane time-harmonic wave of diminishing amplitudes.

For a homogeneous medium obeying the linearity, the causality and the passivity conditions as discussed before, and for a complex wave number $K(\omega)$ defined by eqn (29), it can be shown that the following relationships exist between the real part and the imaginary part of the complex wave number $K(\omega)$:

$$\bar{c}(\omega) = \bar{c}(0)\left[1 + \frac{2\bar{c}(0)\omega^2}{\pi}\int_0^{\infty} \frac{\alpha(\Omega)}{\Omega^2(\Omega^2-\omega^2)}\,\mathrm{d}\Omega\right]^{-1}, \tag{39}$$

$$\alpha(\omega) = -\frac{2\omega^2}{\pi}\int_0^{\infty}\left[\frac{1}{\bar{c}(\Omega)} - \frac{1}{\bar{c}(0)}\right]\frac{\mathrm{d}\Omega}{\Omega^2-\omega^2}, \tag{40}$$

where the integrals should be understood as Cauchy principal value integrals. These relations were first established by Kramers (1927) and Kronig (1926) in the theory of optical dispersion, and they are often referred to as Kramers–Kronig relations. They enable us to calculate the phase velocity $\bar{c}(\omega)$ once the attenuation coefficient $\alpha(\omega)$ is known, or vice versa. Also, to calculate the phase velocity by using eqn (39), knowledge of its static limit $\bar{c}(0)$ is required. This provides no difficulties since $\bar{c}(0)$ is directly related to the static effective stiffness of the damaged solid, which can be found in many works known in the literature. For methods on finding the static effective stiffness of damaged solids see for instance Hutchinson (1987) and references given therein.

Another interesting quantity is the group velocity, denoted by $\bar{c}^{g}$, which differs in general from the phase velocity $\bar{c}$ due to the presence of damages. The group velocity $\bar{c}^{g}$ is related to the phase velocity $\bar{c}$ by (e.g. Achenbach, 1973)

$$\bar{c}^{g} = \bar{c} + k\frac{\mathrm{d}\bar{c}}{\mathrm{d}k}, \tag{41}$$

where k is the wave number of the incident wave. The importance of the group velocity is due to the fact that it equals the energy propagation velocity, which has direct relevance to experimental measurements by using receive transducers. It should be remarked here that in a damaged solid the direction of energy propagation differs from that of wave propagation with the phase velocity. A detailed discussion on this subject is beyond the scope of this paper, and for more detail see Beltzer (1988).

5. DYNAMIC EFFECTIVE STIFFNESS

Having determined the phase velocity $\bar{c}(\omega)$ and the attenuation coefficient $\alpha(\omega)$, the complex wave number $K(\omega)$ can be subsequently computed via eqn (29). Then, the analysis can be proceeded to determine the dynamic effective stiffness $\bar{E}_{ijkl}(\omega)$. To this end, a direct relationship between $\bar{E}_{ijkl}(\omega)$ and $K(\omega)$, or what is equivalent, between $\bar{E}_{ijkl}(\omega)$, $\alpha(\omega)$ and $\bar{c}(\omega)$, is required. Such a relationship can be obtained by substituting the general form of

eqn (30) into equation of motion (2), which yields the following complex Christoffel equation:

$$\left[\Gamma_{ik}(\omega)-\frac{\bar{\rho}\omega^2}{K^2(\omega)}\delta_{ik}\right]U_k(\omega)=0, \tag{42}$$

where

$$\Gamma_{ik}(\omega)=\bar{E}_{ijkl}(\omega)n_jn_l \tag{43}$$

is the symmetric and complex Christoffel stiffness tensor, and n_j are the components of the wave propagation vector $\mathbf{n}$. For non-trivial solutions $U_k(\omega)$ it is necessary to have

$$\det\left[\Gamma_{ik}-\frac{\bar{\rho}\omega^2}{K^2}\delta_{ik}\right]=0. \tag{44}$$

By using the substitution

$$V(\omega)=\frac{\bar{\rho}\omega^2}{K^2(\omega)}, \tag{45}$$

we obtain from (44) a cubic equation of the form

$$V^3-I_1V^2+I_2V-I_3=0, \tag{46}$$

where

$$I_1=\Gamma_{ii},\quad I_2=\tfrac{1}{2}(\Gamma_{ii}\Gamma_{jj}-\Gamma_{ij}\Gamma_{ij}),\quad I_3=\det(\Gamma_{ij}). \tag{47}$$

Explicit solutions to (46) can be obtained as

$$V_1=A+B+\frac{I_1}{3}, \tag{48}$$

$$V_2=-\frac{A+B}{2}+\frac{\sqrt{3}}{2}i(A-B)+\frac{I_1}{3}, \tag{49}$$

$$V_3=-\frac{A+B}{2}-\frac{\sqrt{3}}{2}i(A-B)+\frac{I_1}{3}, \tag{50}$$

in which

$$A=\left[-\frac{b}{2}+\sqrt{\frac{b^2}{4}+\frac{a^3}{27}}\right]^{1/3},\quad B=\left[-\frac{b}{2}-\sqrt{\frac{b^2}{4}+\frac{a^3}{27}}\right]^{1/3}, \tag{51}$$

$$a=I_2-\tfrac{1}{3}I_1^2,\quad b=-\tfrac{1}{27}(2I_1^3-9I_1I_2+27I_3). \tag{52}$$

Substitution of eqns (48)–(50) into (45) results in

$$K_i^2(\omega,\mathbf{n})=\bar{\rho}\omega^2V_i^{-1}\quad i=1,2,3. \tag{53}$$

Equation (53) provides a set of non-linear equations for the components of the dynamic effective stiffness tensor $\bar{E}_{ijkl}(\omega)$, if the effective mass density $\bar{\rho}$, the wave propagation vector $\mathbf{n}$, and the complex wave numbers $K_i(\omega,\mathbf{n})$ are known. It is assumed in this analysis that

the effective mass density $\bar{\rho}$ is independent of frequency ω and it can therefore be determined by a static analysis. For general anisotropy, there are 21 independent stiffness components, and we need hence at least 21 equations corresponding to 21 values of $K_i(\omega, \mathbf{n})$. For transverse isotropy or orthotropy, the number of the independent stiffness components is reduced to 9, and in this case at least 9 equations are required. Note here that it may not be accurate enough, especially in experimental procedures, to have the same number of equations and unknowns. Instead of this, the number of equations or measurements in different directions should significantly exceed the number of the stiffness components to be determined. This gives rise to an overdetermined system of non-linear equations which can be reduced to an optimization problem (e.g. Castagnede and Sachse, 1988). Substantial simplifications exist for isotropy, where we have

$$K_L^2(\omega) = \bar{\rho}\omega^2[\bar{\lambda}(\omega)+2\bar{\mu}(\omega)]^{-1}, \quad K_T^2(\omega) = \bar{\rho}\omega^2\bar{\mu}^{-1}(\omega), \tag{54}$$

in which $\bar{\lambda}(\omega)$ and $\bar{\mu}(\omega)$ are the complex Lamé's constants, and L and T designate the longitudinal and the transverse waves, respectively. Using eqn (54), the dynamic effective Lamé's constants can be expressed as

$$\bar{\lambda}(\omega) = \bar{\rho}\omega^2[K_L^{-2}(\omega)-2K_T^{-2}(\omega)], \tag{55}$$

$$\bar{\mu}(\omega) = \bar{\rho}\omega^2 K_T^{-2}(\omega). \tag{56}$$

By invoking the relation

$$K_L = \frac{\omega}{\bar{c}_L}+i\alpha_L, \quad K_T = \frac{\omega}{\bar{c}_T}+i\alpha_T \tag{57}$$

eqns (55) and (56) can be written as

$$\bar{\lambda}(\omega) = \bar{\rho}\omega^2\left[\left(\frac{\omega}{\bar{c}_L}+i\alpha_L\right)^{-2}-2\left(\frac{\omega}{\bar{c}_T}+i\alpha_T\right)^{-2}\right], \tag{58}$$

$$\bar{\mu}(\omega) = \bar{\rho}\omega^2\left(\frac{\omega}{\bar{c}_T}+i\alpha_T\right)^{-2}. \tag{59}$$

It should be remarked in passing that the complex dynamic effective stiffness tensor $\bar{E}_{ijkl}(\omega)$ also satisfies the Kramers–Kronig relations (e.g. Gross, 1953; Beltzer, 1988; Golden and Graham, 1988). Since these relations are not directly used in this analysis, they are not given here for the sake of brevity.

6. NUMERICAL EXAMPLE

As an example, we consider in this section a damaged solid whose damaged state is caused by a distribution of completely randomly oriented penny-shaped microcracks of the same radius a. The originally undamaged solid is assumed to be homogeneous, isotropic and linearly elastic, and it possesses the Lamé's constants λ and μ as well as the wave velocities c_L and c_T, respectively. The attenuation coefficient $\alpha(\omega, \mathbf{n})$ is first calculated numerically by using a boundary element method developed by Zhang and Gross (1991b). The average attenuation coefficient $\{\alpha(\omega)\}$ is then obtained by taking the spherical average of $\alpha(\omega, \mathbf{n})$ with respect to the crack orientation. Since the damaged solid with randomly oriented microcracks has a macroscopic isotropy, the wave propagation characteristics, i.e. $\{\alpha\}$, $\bar{c}$ and $\bar{c}^s$, are independent of the direction of wave incidence. All numerical calculations have been carried out for a Poisson's ratio $\nu = 1/3$. For convenience, the normalized attenuation coefficient $\bar{\alpha}$ is introduced as

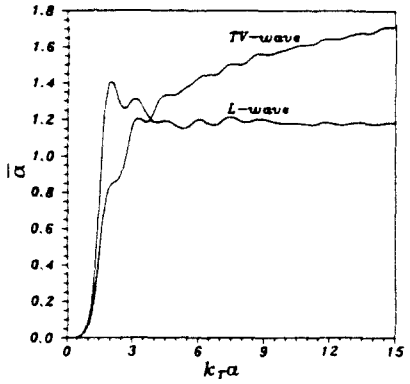

Fig. 3. $\bar{\alpha}$ versus $k_T a$.

$$\tilde{\alpha} = \frac{2a}{\pi\varepsilon}\{\alpha\}, \tag{60}$$

where $\varepsilon = na^3$ represents the crack density parameter.

The variation of the normalized attenuation coefficient $\tilde{\alpha}$ with the dimensionless wave number $k_T a$ is shown in Fig. 3. For incident plane time-harmonic L-waves $\tilde{\alpha}$ first increases rapidly with increasing $k_T a$, and after reaching a peak it then decreases. At high frequencies (large values of $k_T a$) $\tilde{\alpha}$ tends to oscillate about a constant value. For incident plane time-harmonic TV-waves, the variation of $\tilde{\alpha}$ with $k_T a$ is somewhat different. In this case, $\tilde{\alpha}$ increases more or less monotonically with increasing $k_T a$, and no distinct peak is noted, at least in the frequency range considered here.

Figures 4 and 5 show the dependence of the normalized phase velocity $\tilde{c}_L/c_L$ and the normalized group velocity $\tilde{c}_L^g/c_L$ on the dimensionless wave number $k_T a$. The corresponding

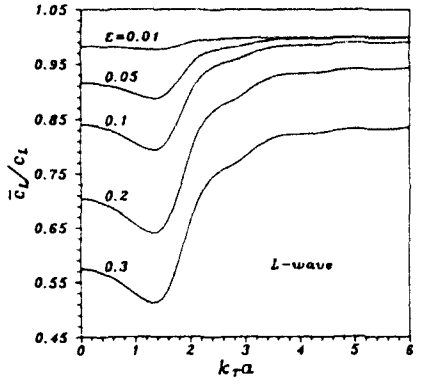

Fig. 4. $\tilde{c}_L/c_L$ versus $k_T a$.

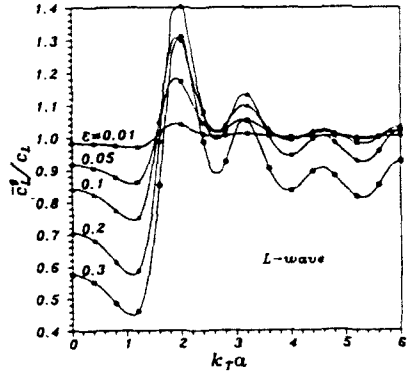

Fig. 5. $\tilde{c}_L^g/c_L$ versus $k_T a$.

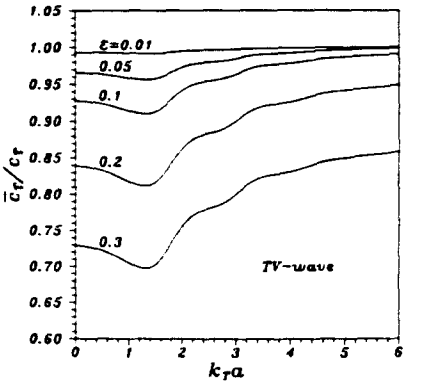

Fig. 6. $\bar{c}_T$ c_T versus k_Ta.

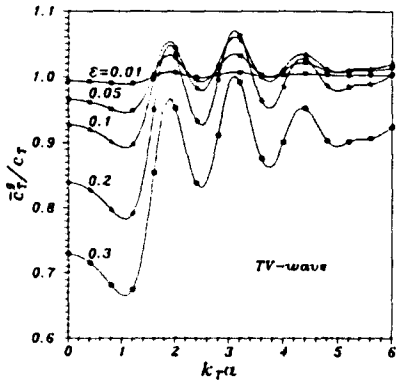

Fig. 7. $\bar{c}_T^g/c_T$ versus k_Ta.

results for $\bar{c}_T/c_T$ are presented in Figs 6 and 7. In the low-frequency range, both $\bar{c}_L/c_L$ and $\bar{c}_T/c_T$ decrease with increasing k_Ta, and after a dip is reached they then increase with further increasing k_Ta. Figures 4 and 6 imply that the phase velocities $\bar{c}_L$ and $\bar{c}_T$ of a damaged solid are smaller than those of the undamaged solid, due to the destructive interaction between the incident waves and the dispersed microcracks. Comparison of Fig. 4 with Fig. 6 shows that for fixed ε and k_Ta, the reduction in $\bar{c}_L$ is generally larger than that in $\bar{c}_T$. For small values of k_Ta, the variations of $\bar{c}_L^g/c_L$ and $\bar{c}_T^g/c_T$ with k_Ta are very similar to those of $\bar{c}_L/c_L$ and $\bar{c}_T/c_T$, while for large values of k_Ta the variations of $\bar{c}_L^g/c_L$ and $\bar{c}_T^g/c_T$ with k_Ta are oscillatory. Depending on the combinations of ε and k_Ta, both the normal dispersion where $\bar{c}_\xi^g > \bar{c}_\xi$ (ξ = L, T) and the anomalous dispersion where $\bar{c}_\xi^g < \bar{c}_\xi$ could occur.

In Figs 8–11, numerical results are presented for the normalized phase velocities $\bar{c}_L/c_L$ and $\bar{c}_T/c_T$, and for the normalized group velocities $\bar{c}_L^g/c_L$ and $\bar{c}_T^g/c_T$, versus the crack density

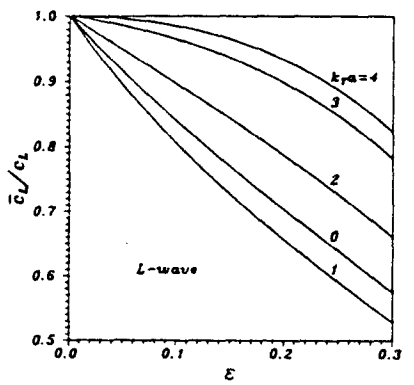

Fig. 8. $\bar{c}_L$ c_L versus ε.

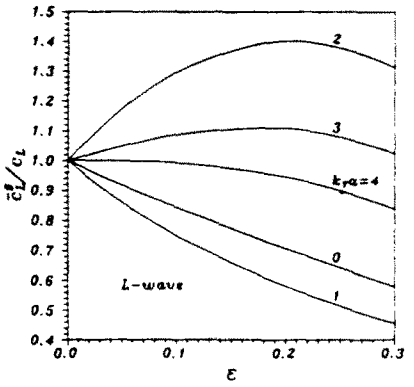

Fig. 9. $\bar{c}_L^g/c_L$ versus ε.

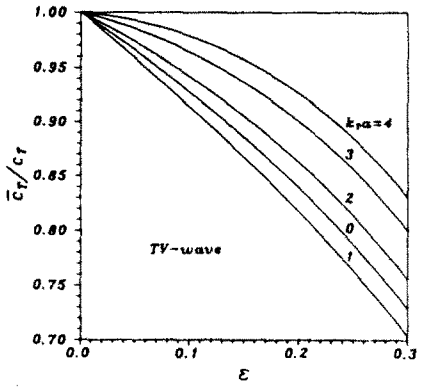

Fig. 10. $\bar{c}_T/c_T$ versus ε.

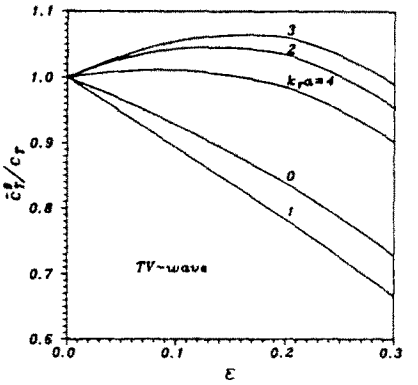

Fig. 11. $\bar{c}_T^g/c_T$ versus ε.

parameter ε. The phase velocities $\bar{c}_L/c_L$ and $\bar{c}_T/c_T$ decrease as ε increases. This tendency is also noted for the group velocities $\bar{c}_L^g/c_L$ and $\bar{c}_T^g/c_T$ at $k_T a = 0$ and $k_T a = 1$, whereas at $k_T a = 2$ and $k_T a = 3$ the group velocities $\bar{c}_L^g/c_L$ and $\bar{c}_T^g/c_T$ first increase with increasing ε, and after reaching their maximum they then decrease with further increasing ε.

The normalized dynamic effective Lamé's constants $\bar{\lambda}/\lambda$ and $\bar{\mu}/\mu$ versus the dimensionless wave number $k_T a$ are shown in Figs 12 and 13. The variations of the real part of $\bar{\lambda}/\lambda$ and $\bar{\mu}/\mu$ with $k_T a$ are similar to those of $\bar{c}_L/c_L$ and $\bar{c}_T/c_T$ given in Figs 4 and 6. Departing from zero, the imaginary part of $\bar{\lambda}/\lambda$ and $\bar{\mu}/\mu$ decreases with increasing $k_T a$ until a local minimum is reached. Thereafter, it shows an oscillatory behavior, and it then increases as $k_T a$ further increases. In all cases considered here, the imaginary part of $\bar{\lambda}/\lambda$ and $\bar{\mu}/\mu$ is always non-positive.

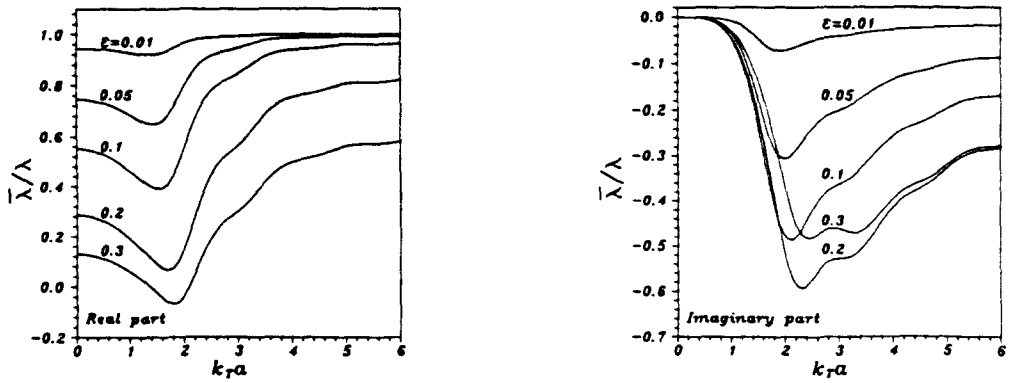

Fig. 12. $\bar{\lambda}/\lambda$ versus $k_T a$.

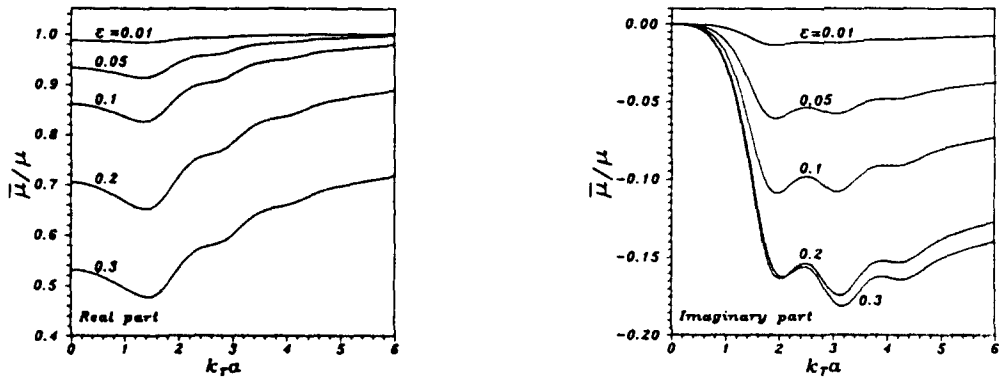

Fig. 13. $\bar{\mu}/\mu$ versus $k_T a$.

Figures 14 and 15 show the effects of the crack density parameter ε on the normalized dynamic effective Lamé's constants $\bar{\lambda}/\lambda$ and $\bar{\mu}/\mu$. For all values of ε considered, the real part of $\bar{\lambda}/\lambda$ and $\bar{\mu}/\mu$ decreases as ε increases. On the other hand, the imaginary part of $\bar{\lambda}/\lambda$ and $\bar{\mu}/\mu$ decreases first with increasing ε until it reaches its minimum. Thereafter, this behavior turns over, and it increases with further increasing ε. The special case $k_T a = 0$ gives the corresponding results for the normalized static effective Lamé's constants $\bar{\lambda}(0)/\lambda$ and $\bar{\mu}(0)/\mu$ where the imaginary part of $\bar{\lambda}/\lambda$ and $\bar{\mu}/\mu$ is identically zero.

Finally, we mention here that the present approach can also be applied to damaged solids with non-randomly oriented microcracks, where the microscopic behavior of the damaged solids is antisotropic. Numerical results for both the attenuation coefficient and

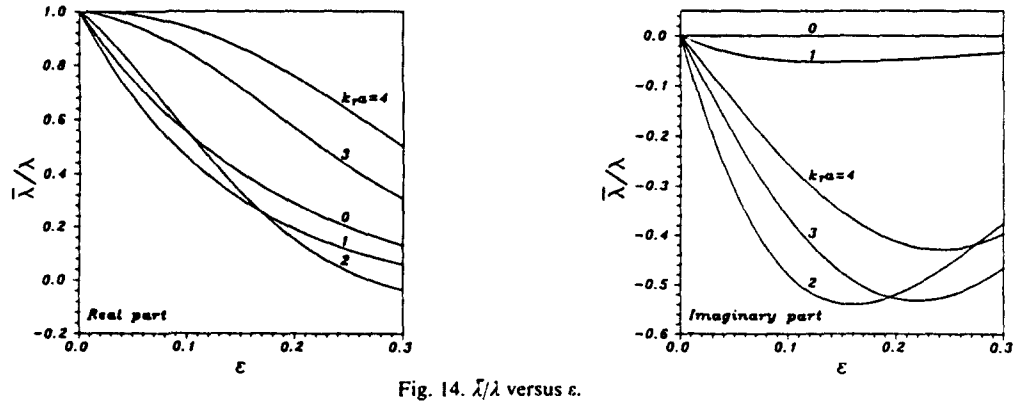

Fig. 14. $\bar{\lambda}/\lambda$ versus ε.

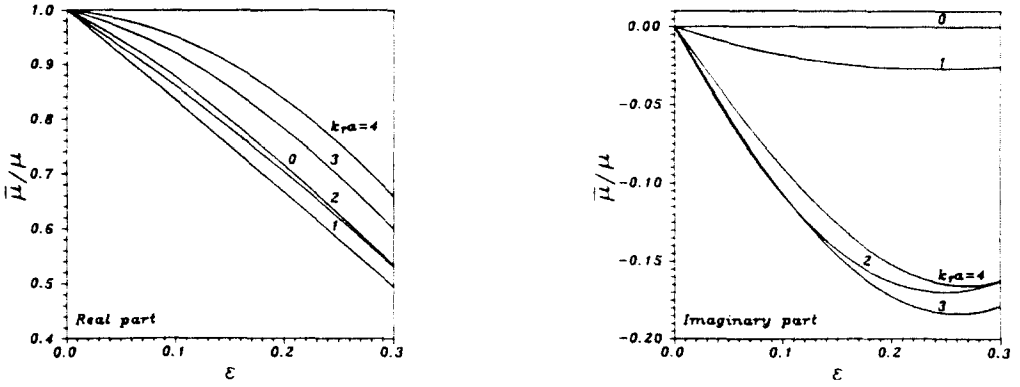

Fig. 15. $\bar{\mu}/\mu$ versus ε.

the phase velocity have been presented by Zhang and Gross (1991a) who took the non-random orientation of microcracks into account. It has been shown therein that for a non-random orientation of microcracks and depending on the crack density parameter ε, the dimensionless wave number $k_T a$, and the direction of wave incidence $\mathbf{n}$, the constructive interaction between elastic waves and dispersed microcracks may dominate the process, unlike for a completely random orientation of microcracks treated here where the destructive interaction prevails. Consequently, the effective wave (phase) velocity of a damaged solid with non-randomly oriented microcracks can even be larger than that of the undamaged solid. Here, it should be mentioned again that the present approach neglects interaction effects among individual cracks, and it is valid only for small damage densities. Future research should be directed to take the interaction effects into account, at least approximately, and to estimate the range of ε in which the present approach is applicable.

REFERENCES

Aboudi, J. (1988). Wave propagation in damaged composite materials. *Int. J. Solids Structures* **24**, 117–138.

Achenbach, J. D. (1973). *Wave Propagation in Elastic Solids*. North-Holland, Amsterdam.

Achenbach, J. D. (1990). From ultrasonics to failure prevention. In *Elastic Waves and Ultrasonic Nondestructive Evaluation* (Edited by S. K. Datta, J. D. Achenbach and Y. S. Rajapakse). North-Holland, Amsterdam.

Anderson, D. L., Minster, B. and Cole, D. (1974). The effects of oriented cracks on seismic velocities. *J. Geophys. Res.* **79**, 4001–4015.

Angel, Y. C. and Achenbach, J. D. (1990). Determination of the effective wave velocity of SH-waves in a cracked solid using the Kramers–Kronig relations. Submitted.

Beltzer, A. I. (1988). *Acoustics of Solids*. Springer-Verlag, New York.

Beltzer, A. I. (1989). The effective dynamic response of random composites and polycrystals—a survey of the causal approach. *Wave Motion* **11**, 211–229.

Bose, S. K. and Mal, A. K. (1974). Elastic waves in fiber-reinforced composites. *J. Mech. Phys. Solids* **22**, 217–229.

Castagnede, B. and Sachse, W. (1988). Optimized determination of elastic constants of anisotropic solids from wavespeed measurements. In *Review of Quantitative Nondestructive Evaluation* (Edited by D. O. Thompson and D. E. Chimenti), Vol. 8B, pp. 1855–1862. Plenum Press, New York.

Chatterjee, A. K., Mal, A. K., Knopoff, L. and Hudson, J. A. (1980). Attenuation of elastic waves in a cracked, fluid-saturated solid. *Math. Proc. Camb. Phil. Soc.* **88**, 547–561.

Datta, S. K., Ledbetter, H. M., Shindo, Y. and Shah, A. H. (1988). Phase velocity and attenuation of plane elastic waves in a particle-reinforced composite medium. *Wave Motion* **10**, 171–182.

Foldy, L. L. (1949). Multiple scattering theory of waves. *Phys. Rev.* **67**, 107–119.

Golden, J. M. and Graham, G. A. (1988). *Boundary Value Problems in Linear Viscoelasticity*. Springer-Verlag, New York.

Gross, B. (1953). *Mathematical Structures of the Theories of Viscoelasticity*. Hermann, Paris.

Gubernatis, J. E. and Domany, E. (1984). Effects of microstructure on the speed and attenuation of elastic waves in porous materials. *Wave Motion* **6**, 579–589.

Hudson, J. A. (1981). Wave speeds and attenuation of elastic waves in material containing cracks. *Geophys. J. R. Astr. Soc.* **64**, 133–150.

Hudson, J. A. (1986). A higher order approximation to the wave propagation constants for a cracked solid. *Geophys. J. R. Astr. Soc.* **87**, 265–274.

Hutchinson, J. W. (1987). Micro-mechanics of damage in deformation and fracture. Department of Solid Mechanics, Technical University of Denmark.

Kinra, V. K. and Anaud, A. (1982). Wave propagation in a random particulate composite at long and short wavelengths. *Int. J. Solids Structures* **18**, 367–380.

Kinra, V. K., Petraitis, M. S. and Datta, S. K. (1976). Ultrasonic wave propagation in a random particulate composite. *Int. J. Solids Structures* **16**, 301–312.
Kramers, H. A. (1927). La diffusion de la lumière par les atomes. *Estratto dagli Atti del Congresso Internazionale de Fisica Coma* 2, pp. 545–557.
Kronig, R. L. (1926). On the theory of dispersion of X-rays. *J. Opt. Soc. Amer.* **12**, 547–557.
Kuster, G. T. and Toksoz, M. N. (1974). Velocity and attenuation of seismic waves in two-phase media: Part I and Part II. *Geophysics* **39**, 587–618.
Lax, M. (1952). Multiple scattering of waves II. Effective field in dense systems. *Phys. Rev.* **85**, 621–629.
Ledbetter, H. M. and Datta, S. K. (1986). Effective wave speeds in an SiC-particle-reinforced Al composite. *J. Acoust. Soc. Amer.* **79**, 239–248.
Lewandowski, J. (1987a). Acoustic waves in solids with random cavities, I: Effective macroscopic parameters. *Acta Mech.* **68**, 1–20.
Lewandowski, J. (1987b). Acoustic waves in solids with random cavities, II: Energy density considerations. *Acta Mech.* **68**, 21–32.
Mal, A. K. and Knopoff, L. (1967). Elastic wave velocities in two-component systems. *J. Inst. Math. Applicns* **3**, 376–387.
McCarthy, M. F. and Carroll, M. M. (1984). Wave propagation in randomly cracked media. In *Wave Propagation in Homogeneous Media and Ultrasonic Nondestructive Evaluation* (Edited by G. C. Johnson), Vol. 62, pp. 141–153. ASME, New York.
McCoy, J. J. (1973). On the dynamic response of disordered composites. *J. Appl. Mech.* **40**, 511–517.
O'Connell, R. J. and Budiansky, B. (1974). Seismic velocities in dry and saturated cracked solids. *J. Geophys. Res.* **79**, 5412–5426.
Piau, M. (1979). Attenuation of plane compressional wave by a random distribution of thin circular cracks. *Int. J. Engng Sci.* **17**, 151–167.
Piau, M. (1980). Crack-induced anisotropy and scattering in stressed rocks: effective elastic moduli and attenuation. *Int. J. Engng Sci.* **18**, 549–568.
Sabina, F. J. and Willis, J. R. (1988). A simple self-consistent analysis of wave propagation in particulate composites. *Wave Motion* **10**, 127–142.
Sayers, C. M. (1980). On the propagation of ultrasound in highly concentrated mixtures and suspensions. *J. Phys. D: Appl. Phys.* **13**, 179–184.
Sayers, C. M. (1981). Ultrasonic velocity in porous materials. *J. Phys. D: Appl. Phys.* **14**, 413–420.
Sayers, C. M. and Smith, R. L. (1981). The propagation of ultrasound in porous media. *Ultrasonics* **20**, 201–205.
Sayers, C. M. and Smith, R. L. (1983). Ultrasonic velocity and attenuation in an epoxy matrix containing lead inclusions. *J. Phys. D: Appl. Phys.* **16**, 1189–1194.
Stigh, U. (1987). Influence of damage on ultrasonic velocity and strength—analysis and experiments. *Engng Fract. Mech.* **28**, 1–12.
Varadan, V. K. and Varadan, V. V. (1979). Frequency dependence of elastic (SH-) wave velocity and attenuation in anisotropic two phase media. *Wave Motion* **1**, 53–56.
Varadan, V. K., Ma, Y. and Varadan, V. V. (1985). A multiple scattering theory for elastic wave propagation in discrete random medium. *J. Acoust. Soc. Am.* **77**, 375–385.
Varadan, V. K., Varadan, V. V. and Pao, Y. H. (1978). Multiple scattering of elastic waves by cylinders of arbitrary cross sections. I. SH-waves. *J. Acoust. Soc. Amer.* **63**, 1310–1319.
Zhang, C. H. and Achenbach, J. D. (1990). Dispersion and attenuation of surface waves due to distributed surface-breaking cracks. *J. Acoust. Soc. Amer.* **88**, 1986–1992.
Zhang, C. H. and Achenbach, J. D. (1991). Effective wave velocity and attenuation in a material with distributed penny-shaped cracks. *Int. J. Solids Structures* **27**, 751–767.
Zhang, C. H. and Gross, D. (1991a). Attenuation and dispersion of elastic waves in randomly cracked solids. Submitted to *J. Mech. Phys. Solids*.
Zhang, C. H. and Gross, D. (1991b). 3-D elastodynamic crack analysis by a non-hypersingular BIEM. Accepted for publication in *Computational Mech.*